Elastic constants of diamond from molecular dynamics simulations

2006 J. Phys.: Condens. Matter 18 S1737

(http://iopscience.iop.org/0953-8984/18/32/S05)

INSTITUTE OF PHYSICS PUBLISHING JOURNAL OF PHYSICS: CONDENSED MATTER

J. Phys.: Condens. Matter **18** (2006) S1737–S1750 doi:10.1088/0953-8984/18/32/S05

Elastic constants of diamond from molecular dynamics simulations

Guangtu Gao, Kevin Van Workum, J David Schall and Judith A Harrison[1]

Department of Chemistry, United States Naval Academy, Annapolis, MD 21402, USA

E-mail: jah@usna.edu

Received 19 December 2005
Published 24 July 2006
Online at stacks.iop.org/JPhysCM/18/S1737

Abstract

The elastic constants of diamond between 100 and 1100 K have been calculated for the first time using molecular dynamics and the second-generation, reactive empirical bond-order potential (REBO). This version of the REBO potential was used because it was redesigned to be able to model the elastic properties of diamond and graphite at 0 K while maintaining its original capabilities. The independent elastic constants of diamond, C_{11}, C_{12}, and C_{44}, and the bulk modulus were all calculated as a function of temperature, and the results from the three different methods are in excellent agreement. By extrapolating the elastic constant data to 0 K, it is clear that the values obtained here agree with the previously calculated 0 K elastic constants. Because the second-generation REBO potential was fit to obtain better solid-state force constants for diamond and graphite, the agreement with the 0 K elastic constants is not surprising. In addition, the functional form of the second-generation REBO potential is able to qualitatively model the functional dependence of the elastic constants and bulk modulus of diamond at non-zero temperatures. In contrast, reactive potentials based on other functional forms do not reproduce the correct temperature dependence of the elastic constants. The second-generation REBO potential also correctly predicts that diamond has a negative Cauchy pressure in the temperature range examined.

(Some figures in this article are in colour only in the electronic version)

1. Introduction

Diamond has many unique properties due to its tetrahedrally coordinated covalent bonds [1, 2]. These properties include very large elastic modulus, high sound velocities, high Debye

[1] Author to whom any correspondence should be addressed.

temperature (2340 K) [3], large thermal conductivity, low wear rate, and low friction [1, 2, 4–6]. Because of diamond's unique friction and wear properties, there have been a number of experimental [2, 5, 7–19] and theoretical studies [20–29] that have investigated the friction of diamond and diamond-like carbon films. Diamond-like carbon describes hydrogenated and hydrogen-free metastable amorphous carbon materials, prepared by a variety of plasma vapour deposition and chemical vapour deposition (CVD) techniques. These films possess a wide range of mechanical and tribological properties [2].

Diamond-like carbon, and other solid lubricants, may prove useful in a number of applications, such as space-based technologies and microelectromechanical systems, where liquid lubrication is not feasible [30–35]. Solid lubricants used in space-based technologies would experience harsh environments and large temperature fluctuations. Temperature fluctuations will lead to changes in material properties, such as thermal conductivity, electrical conductivity, elastic properties, plastic flow, surface diffusion and viscosity. In addition, these material properties may also influence tribological behaviour. Thus, the temperature dependence of the material and tribological properties of solid lubricants for space-based applications needs to be elucidated.

Molecular dynamics (MD) simulations are uniquely suited to study the effects of temperature on material and tribological properties due to the explicit inclusion of temperature. This work is aimed at elucidating the temperature dependence of the elastic constants of diamond using MD simulations. Intramolecular forces are modelled using the second-order reactive empirical bond-order potential (REBO) [37, 38]. The REBO potential energy function is a many-body function that is capable of modelling all the hybridization states of carbon and is, therefore, able to model chemical reactions that may accompany sliding.

Diamond was selected as the first material to be examined for two reasons. First, the elastic constants of diamond as a function of temperature have been experimentally determined using Brillouin scattering [1]. Thus, a comparison of experimentally and computationally determined values is possible. Second, we have calculated the elastic constants using three computational techniques. These are the direct method [39], the strain-fluctuation method [40, 41], and the stress-fluctuation method [42–47]. The stress-fluctuation method can provide insight into the molecular origin of a given mechanical response and this method converges more rapidly than the strain-fluctuation method [47]. However, implementation of this method is challenging for a complex, many-body potential, such as the REBO potential. Because diamond contains carbon in one hybridization state, this simplifies the initial implementation of the stress-fluctuation method.

2. Method

Brenner originally developed the REBO potential to model the CVD growth of diamond [48, 49]. Since its inception, it has been used extensively to model diamond growth [50], the tribology of diamond surfaces [22–28], carbon nanotubes [52], carbon clusters [53], and scattering of fullerenes from diamond surfaces [54]. Recently, Brenner and co-workers developed the second-generation REBO potential [37, 38]. This improved form of the hydrocarbon potential includes both modified analytic functions for the intramolecular interactions and an expanded fitting database. This new function yields a much improved description of bond energies, bond lengths, and force constants for carbon–carbon bonds compared to the original REBO potential. Thus, this potential has an improved fit to the 0 K elastic properties of diamond and graphite which, in turn, yields better predictions for the energies of several surface reconstructions and interstitial defects. Forces associated with the rotation about dihedral angles for carbon–carbon double bonds and angular interactions

associated with hydrogen centres, absent from the original REBO, are also included in the second-generation REBO [37, 38, 77]. This revised potential has been successful in modelling a wide range of processes, such as cluster dynamics [55, 56], nanotube properties [51, 57], polycrystalline diamond structures [58–60], and the tribology of amorphous carbon surfaces [20, 21].

Because the second-generation REBO potential is able to quantitatively reproduce the 0 K elastic constants of diamond and graphite, we adopt it in this current study of the non-zero temperature elastic constants. Both versions of the REBO potential take the simple functional form [37, 38, 48, 49]

$$U = \tfrac{1}{2}\sum_{\alpha,\beta}[V_{\mathrm{R}}(r_{\alpha\beta}) - B_{\alpha\beta}V_{\mathrm{A}}(r_{\alpha\beta})], \tag{1}$$

where V_{R} and V_{A} represent two-body repulsive and attractive interactions, respectively. It should be noted, however, that the analytic forms of both V_{R} and V_{A} were changed in the second-generation REBO potential [37, 38]. The term $B_{\alpha\beta}$ is a many-body, bond-order term which is a function of bond angles, torsional angles, bond lengths, and atomic coordination in the vicinity of the bond between atoms α and β. A more detailed description of the second-generation REBO potential and its parameters is given elsewhere [37, 38, 77].

Interatomic interaction forces in the REBO potential are derived not only from the two-body terms, V_{R} and V_{A}, but also from the many-body bond-order term, $B_{\alpha\beta}$. This gives the REBO potential the capability to model all the possible hybridization states of carbon. This potential can be written as a function of interatomic distances and we show in the appendix that the internal stress tensor of the system can be calculated using a formula similar to that for a two-body potential. The internal stress tensor is given by

$$\sigma_{ij} = \frac{1}{V}\left(\sum_{\alpha} m_\alpha v_{\alpha i} v_{\alpha j} + \sum_{(\alpha<\beta)} r_{\alpha\beta i} f_{\alpha\beta j}\right), \tag{2}$$

where σ_{ij} is the ij component of the stress tensor, V is the volume of the system, m_α and v_α are mass and velocity of atom α, respectively, $r_{\alpha\beta i}$ is the Cartesian component of the vector from atom β to atom α in the i direction, and $f_{\alpha\beta j}$ is the force acting on atom α by atom β in the j direction. (Here we adopt the convention that the Latin subscripts i, j, and k refer to Cartesian coordinates (x, y, and z) and the Greek subscripts α and β refer to atomic indices.)

There are two basic methods of calculating elastic constants from molecular dynamics simulations. These are a direct method [36], which derives elastic constants from the stress–strain curve, and fluctuation methods [36, 40, 43–45, 61–67], which use ensemble averages of the fluctuations in either strain or stress. The basic relation between stress and strain is given by Hooke's law:

$$\sigma_{ij} = \sum_{k,l} C_{ijkl}\epsilon_{kl}, \tag{3}$$

where C_{ijkl} represents the fourth-rank elastic stiffness tensor and ϵ_{kl} is the kl element of the second-rank strain tensor. The fourth-rank elastic stiffness tensor can be converted to a 6×6 matrix [39]. To convert from tensor notation to matrix notation, a pair of indices is converted to a single number using the following rules: $11 \rightarrow 1$, $22 \rightarrow 2$, $33 \rightarrow 3$, 23 and $32 \rightarrow 4$, 13 and $31 \rightarrow 5$, and 12 and $21 \rightarrow 6$. Furthermore, in matrix notation the indices 1, 2, and 3 map to x, y, and z, respectively. For crystals with cubic symmetry, such as diamond, there are only three independent elastic constants, which are C_{11}, C_{12}, and C_{44}.

The basic equation employed in the strain-fluctuation method is [40, 41]

$$\langle\epsilon_{ij}\epsilon_{kl}\rangle - \langle\epsilon_{ij}\rangle\langle\epsilon_{kl}\rangle = \frac{k_{\mathrm{B}}T}{V}S_{ijkl}, \tag{4}$$

where k_B is the Boltzmann constant, S_{ijkl} is the elastic compliance tensor, which is the inverse of the elastic stiffness tensor, and $\langle\,\rangle$ represents an ensemble average in a constant enthalpy, thermodynamic tension, and particle number (HtN) ensemble [43], or a constant temperature, thermodynamic tension, and particle number (TtN) ensemble [44]. In these simulations, the computational cell is allowed to change size and shape according to the method of Parrinello and Rahman [68]. In variable shape and size MD simulations, the shape of the simulation cell is a dynamic variable. The simulation cell is constructed from three time-dependent vectors **a**, **b**, and **c**. The matrix h is formed from these time-dependent vectors such that $h = (\mathbf{a}, \mathbf{b}, \mathbf{c})$. The relationship between the instantaneous strain tensor ϵ and the h matrix is [40]

$$\epsilon_{ij} = \frac{1}{2}\left[\left(h_0^{-1}\right)^{\mathrm{T}}_{im} h^{\mathrm{T}}_{mn} h_{np} \left(h_0^{-1}\right)_{pj} - \delta_{ij}\right], \tag{5}$$

where h_0 is the h matrix of the reference system, and the superscript T stands for the transpose of a matrix. For detailed explanations of (H, t, N) and (T, t, N) ensembles, readers are referred to the original works of Parrinello and Rahman [41, 68], and Ray and Rahman [43, 44].

Elastic constants at non-zero temperatures can also be calculated using the stress-fluctuation method [40, 43, 44]:

$$C_{ijkl} = \langle C^B_{ijkl}\rangle - \frac{V}{k_B T}(\langle\sigma_{ij}\sigma_{kl}\rangle - \langle\sigma_{ij}\rangle\langle\sigma_{kl}\rangle) + C^K_{ijkl}, \tag{6}$$

where C^B_{ijkl} is the Born term,

$$C^B_{ijkl} = \frac{1}{V}\frac{\partial^2 U}{\partial\epsilon_{ij}\partial\epsilon_{kl}}, \tag{7}$$

which is used to determine the elastic constants at 0 K, and C^K_{ijkl} is the kinetic term

$$C^K_{ijkl} = \frac{2Nk_B T}{V}(\delta_{ik}\delta_{jl} + \delta_{il}\delta_{jk}). \tag{8}$$

With the stress-fluctuation method, the simulation is performed under a constant volume constraint. Therefore, adiabatic elastic constants can be obtained with a microcanonical ensemble (NVE) simulation, and isothermal elastic constants can be obtained with a canonical ensemble simulation.

It has been shown that the stress-fluctuation method converges better than the strain-fluctuation method [63]. Implementation of the stress-fluctuation method requires evaluation of the Born term, or evaluation of the second derivative of the potential energy function with respect to strain. For a many-body potential, such as the REBO potential, evaluation of this term is challenging. We have been able to derive the analytical form of the REBO potential's Born term, and the results will be published elsewhere [69].

The third method used here to calculate the elastic constants as a function of temperature is a direct method. In general, to calculate elastic constants using a direct method, computer simulations are performed in either a constant strain or a constant stress condition, and the corresponding stress or strain is obtained from the ensemble average. If a constant stress is applied, the simulation box should be allowed to change both its size and shape to obtain the ensemble average of the corresponding strain. In this case, the (HtN) ensemble or (TtN) ensemble techniques must be used [36].

The direct method used here is based on a constant-volume simulation in an orthorhombic simulation cell. The simulation cell is constructed such that each of the edge vectors of the cell is parallel with an edge of the unit cell of the diamond lattice. If the simulation box is scaled in the x direction by a factor $1 - e$, where e is known as the compression ratio, then the system is under a strain $\epsilon_{xx} = e$, for small values of e. Therefore, we have the following relations:

$$\sigma_{xx} = C_{11}e \tag{9}$$

and

$$\sigma_{yy} + \sigma_{zz} = 2C_{12}e. \tag{10}$$

Using a constant volume simulation, the corresponding stresses, σ_{xx}, σ_{yy}, and σ_{zz}, given in equation (2), can be obtained from the ensemble averages and C_{11} and C_{12} can be calculated with equations (9) and (10).

One more equation relating strain and stress is required to calculate C_{44}. It can be shown using equation (5) that compressing the crystal structure along the [110] lattice direction by a factor $1 - e$ is equivalent to the strain conditions $\epsilon_{xx} = \epsilon_{yy} = e/2$ and $\epsilon_{xy} = e$. Therefore,

$$\sigma_{xx} + \sigma_{yy} = (C_{11} + C_{12})e, \tag{11}$$

and

$$\sigma_{xy} = C_{44}e. \tag{12}$$

σ_{xy} can be obtained directly from an ensemble average in a constant volume situation. An additional complication arises when applying this strain to the cubic unit cell. That is, it will cause the simulation box to become non-orthorhombic, and require additional effort in handling the periodic boundary conditions. With this in mind, we choose an orthorhombic simulation cell, in which the [110] direction of the crystal lattice is set to be parallel with an edge of the cell. It can be shown that pressure on an imaginary plane perpendicular to the [110] direction, P_{110}, is given by

$$P_{110} = \tfrac{1}{2}(C_{11} + C_{12} + 2C_{44})e. \tag{13}$$

The pressure, P_{110}, can be obtained in a constant-volume simulation. Thus, the three independent elastic constants of a cubic crystal can be calculated by directly applying a strain to the simulation box and making use of equations (9), (10), and (13).

In most of the simulations reported here, the simulation system contains 1000 carbon atoms. Dynamic equations are integrated using the fourth-order Gear predictor–corrector algorithm with a constant step size of 0.25 fs [70]. Temperatures are controlled using Nose's extended-system method [71].

3. Results

Both the direct and the stress-fluctuation methods require the simulations to be conducted in a canonical (NVT) ensemble. Because the lattice parameter of diamond is dependent upon temperature, this dependence must be determined to ensure that all simulations are done under the zero-pressure condition. For this reason, a series of constant pressure MD simulations were conducted. In these simulations, the external pressure is set to zero and controlled with Andersen's extended-system method [72] while the volume of the box is allowed to uniformly change. After equilibration, the volume of the box at that temperature is obtained. The lattice constants obtained using this method are shown as a function of temperature in figure 1. Thewlis and Davey studied the thermal expansion of both industrial and gem-quality diamond from 123 to 1223 K [73]. For comparison, their results for gem-quality diamond are also shown in figure 1. At 0 K, the calculated lattice parameter of diamond is nearly identical to the experimental value. This is largely due to the fact that the 0 K properties of diamond were used to obtain the parameters for the second-generation REBO potential [37, 38]. At non-zero temperatures, the second-generation REBO potential predicts that the lattice parameter of diamond increases almost linearly with increasing temperature. This trend agrees qualitatively with the experimentally determined values at non-zero temperatures. However, the experimentally determined lattice constants do not have as strong a linear temperature

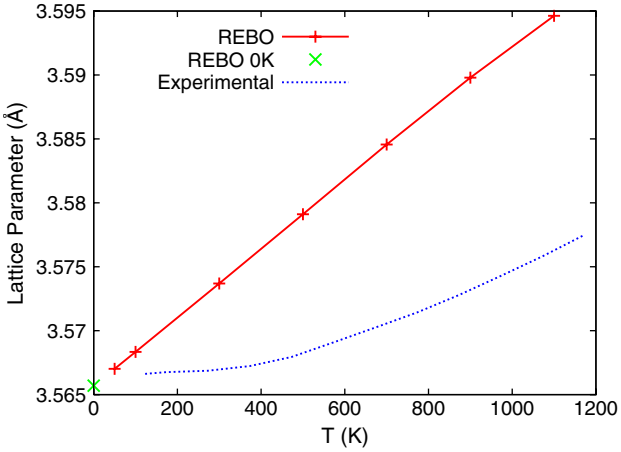

Figure 1. Lattice parameter of diamond as a function of temperature calculated using the second-generation REBO potential energy function. Experimental values are shown for comparison.

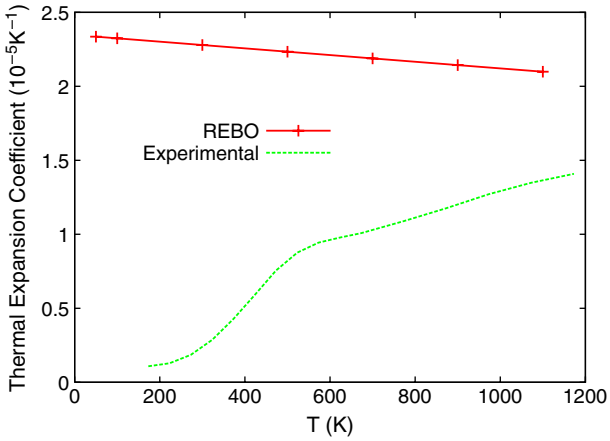

Figure 2. Thermal expansion coefficient as a function of temperature calculated using the second-generation REBO potential. Experimental values are shown for comparison.

dependence compared to the simulation results. The lack of quantitative agreement between the calculated and experimentally determined lattice constants at non-zero temperatures indicates that the thermal expansion coefficient, $\alpha = \frac{1}{V}(\frac{\partial V}{\partial T})_P$, of diamond is not accurately predicted by the MD simulations. The thermal expansion coefficients calculated from MD simulations and the corresponding experimental values [73] are shown in figure 2. The calculated data are all larger than the experimental values, and decrease almost linearly from 2.3×10^{-5} to 2.1×10^{-5} K^{-1} as the temperature increases. In contrast, the experimental data approach zero at 0 K, increase nonlinearly with temperature when the temperature is below 600 K, and increase almost linearly above this temperature. In addition, the experimental values of α shown in figure 2 are all below 1.4×10^{-5} K^{-1}. These discrepancies between the experimental and simulated data are largely due to the high Debye temperature of diamond. In fact, it has been shown by the quantum statistical theory that the thermal expansion coefficient is approximately proportional to T^3 at very low temperatures [74]. This quantum effect cannot be predicted by classical MD simulations.

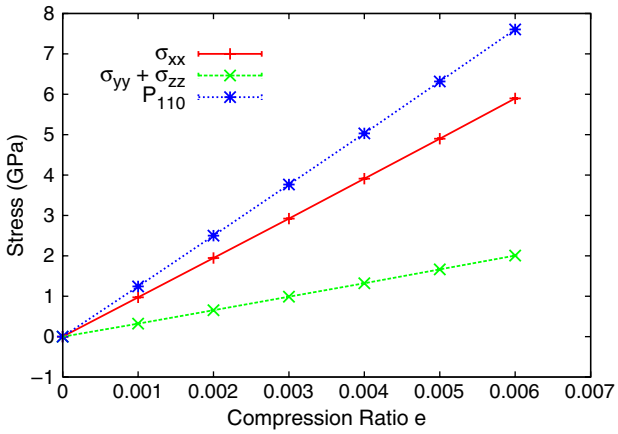

Figure 3. Stress as a function of compression ratio e computed using the direct method described in the text.

A reference system at each temperature was constructed using the calculated values of the lattice parameter. Using the direct method described above, compressions were applied to the reference systems using various values of e. Strains of less than 0.01 were used to ensure that the system was in the region where Hooke's law is satisfied. MD simulations in the canonical ensemble were carried out with the strained systems. The simulation times were approximately 100 ps, or ≈400 000 time steps. The stress tensor for each strained system was then calculated from the ensemble average (equation (2)). Figure 3 shows a typical linear dependence of σ_{xx}, $\sigma_{yy} + \sigma_{zz}$, and P_{110} on the compression ratio e. The elastic constants were then calculated from the strain–stress relationships described above.

The strain-fluctuation method was performed in the (TtN) ensemble, in which the thermodynamic tension t and the external hydrostatic pressure are set to zero. The size and the shape of the simulation system are controlled using the method developed by Parrinello and Rahman [41]. A technique suggested by Nose and Klein [75] is applied to maintain the symmetry of the h matrix, which prevents system rotations. The instantaneous values of the h matrix are averaged over the course of the simulation to obtain h_0. The instantaneous values of the h matrix are also used in the calculation of the instantaneous strain tensor (equation (5)). With these values of instantaneous strain, the elastic constants can be calculated using equation (4). Fluctuations of the three sets of symmetry-equivalent elastic constants C_{11}, C_{22}, C_{33}; C_{12}, C_{13}, C_{23}; and C_{44}, C_{55}, C_{66}, for diamond at 300 K are shown in figure 4. It is clear from analysis of these data that this method is slow to converge. In fact, the slow convergence of this method has been previously documented [76]. In the simulations presented here, it took 5 ns for the symmetry-equivalent elastic constants at 300 K to converge. In addition, we were unable to obtain reliable data at 100 K using this method. At temperatures above 100 K, it is possible to obtain results with acceptable accuracy as long as the simulation is run for a sufficiently long time.

Like the direct method, the stress-fluctuation method is performed in the (NVT) ensemble. The terms in equation (6) are obtained from the MD simulations. As has been previously shown [76], the Born term normally converges very well, and most of the simulation time is used to obtain the stress fluctuation term (middle term in equation (6)). Accurate values of stress fluctuation term can be obtained after approximately 400 000 time steps. These two contributions to the stress are shown in figure 5 as a function of temperature. The kinetic term contributes a negligible amount to the total elastic constant and is not shown. It is clear from

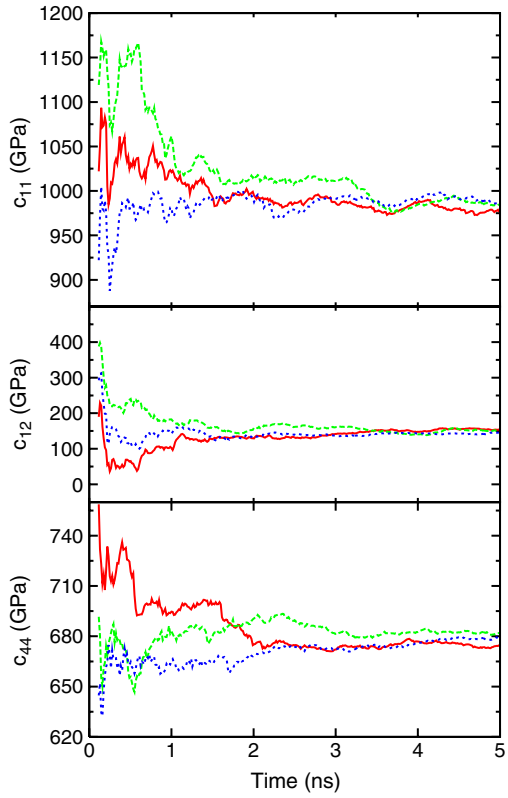

Figure 4. Elastic constants of diamond at 300 K as a function of time calculated using the strain-fluctuation method. In each panel, the red, green, and blue lines represent the symmetry-equivalent elastic constants. For example, in the upper panel, the solid (red), dashed (green) and dotted (blue) lines represent C_{11}, C_{22}, and C_{33}, respectively. C_{12}, C_{21}, and C_{32} are shown in the middle panel and C_{44}, C_{55}, and C_{66} are shown in the lower panel.

analysis of these data that the Born term is the largest contributor to the elastic constants at non-zero temperatures. This lends insight into the fact that the stress-fluctuation method is a much more effective way to calculate the elastic constants than the strain-fluctuation method.

The elastic constants for diamond as a function of temperature calculated with the methods described here are all shown in figure 6. Values obtained using all three methods are all in excellent agreement. In addition, by extrapolating the curves to 0 K, it is clear that these values agree reasonably well with the previously published 0 K elastic constants [37, 77]. It should be noted, however, that there is not quantitative agreement between the experimentally determined and the calculated values of the elastic constants at non-zero temperatures [1]. For example, the calculated values of C_{11} decrease as a function of temperature more markedly than the experimental values with the differences between the two becoming larger at larger temperatures. The experimentally determined values and the calculated C_{44} values also decrease with increasing temperature. However, because the calculated value of C_{44} at 0 K is larger than the experimental value, the calculated values of C_{44} actually get closer to the experimental values as the temperature is increased. Thus, the second-generation REBO potential predicts the correct qualitative trends with temperature for both C_{11} and C_{44}. In contrast, this potential does not predict the correct qualitative trend with temperature for

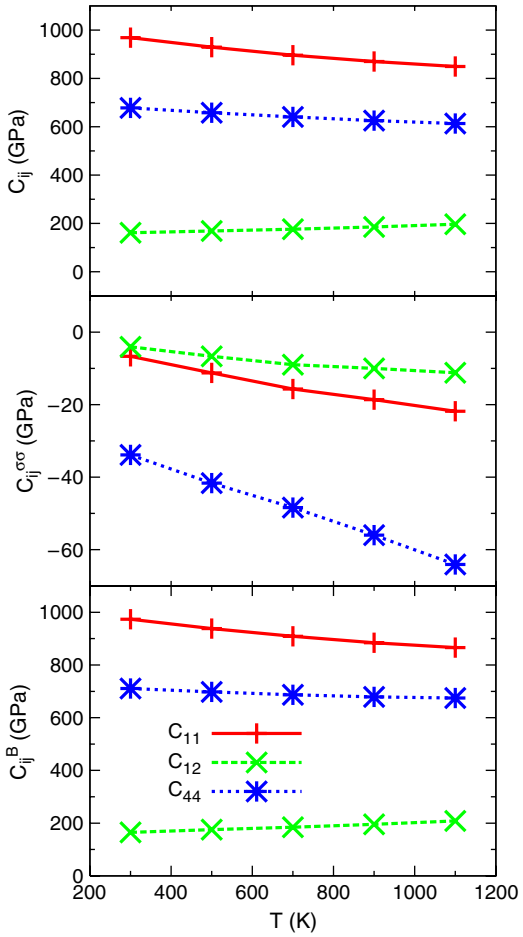

Figure 5. Contributions to the elastic constants of diamond calculated using the stress-fluctuation method. Contributions to the elastic constants from the Born term and from the stress fluctuations are shown in the lower and middle panels, respectively. The total elastic constants calculated using equation (6) are shown in the upper panel.

C_{12}. The experimentally determined values change little, perhaps decreasing slightly, in the temperature range examined while the calculated values increase slightly.

The poor agreement of the calculated C_{12} values with the experimental data, combined with the fast softening of C_{11}, result in bulk moduli that agree fairly well with the experimental values. The bulk modulus for cubic crystals is calculated from the elastic constants using the expression $B = \frac{1}{3}(C_{11} + 2C_{12})$. The calculated and experimental [1] values of bulk moduli for diamond are shown as a function of temperature in figure 7.

The calculated values of bulk moduli are in reasonable agreement with the experimental values, though they decrease slightly more quickly, and the correct qualitative change with temperature is reproduced. The large decrease of the elastic constants C_{11} and C_{44} with increasing temperature predicted by the MD simulations is the direct consequence of the large thermal expansion coefficient obtained from the classical MD simulation. These results are described by Grüneisen's law [78], which states that the higher the thermal expansion coefficient, the faster the elastic softening.

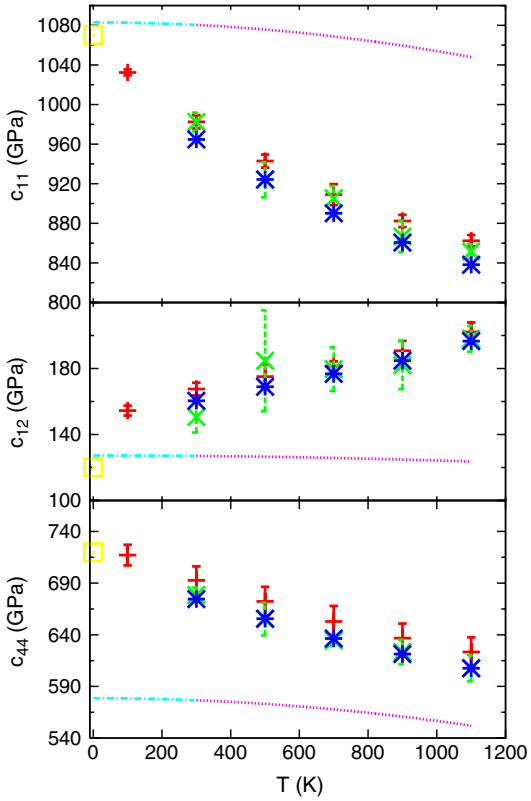

Figure 6. Elastic constants of diamond calculated using MD simulations as a function of temperature. Yellow squares represent the previously published values at 0 K calculated from phonon dispersion relations. Red (plus signs), green (crosses), and blue (asterisks) symbols represent values calculated with the direct, strain-fluctuation, and stress-fluctuation methods, respectively. The pink lines represent the values determined experimentally between 300 and 1600 K using Brillouin scattering. The cyan lines are extrapolations of the experimental data [1].

The second-generation REBO potential correctly predicts the negative Cauchy pressure ($C_{12} - C_{44}$) of diamond at all temperatures (figure 8). This quantity is important for a potential energy function to predict the correct shear deformations in materials. Clearly, if friction is to be studied, the potential energy function should capture the correct response of the material to shear. For a potential energy function to predict the correct Cauchy relationship, the directionality of the bonds must be considered. Potential energy functions that consider pairs of atoms (two-body potentials), such as Lennard-Jones or the embedded atom potential, do not predict the correct Cauchy pressures. Because the REBO potential takes into account the directionality of bonds, via its multi-body formalism, it correctly predicts that diamond has a negative Cauchy pressure over the entire temperature range examined.

4. Summary

Both the stress- and the strain-fluctuation methods are convenient ways to calculate elastic constants as a function of temperature. The stress-fluctuation method is more attractive than the strain-fluctuation method because it converges more quickly and all of the components of the stress tensor are obtained from a single simulation. However, the stress-fluctuation

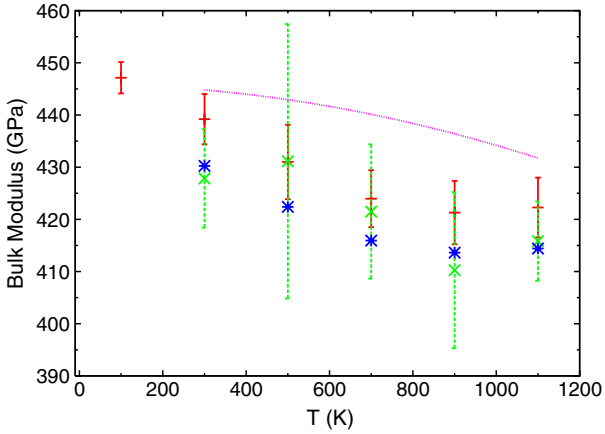

Figure 7. Bulk modulus of diamond as a function of temperature. Moduli values are calculated from the calculated elastic constants using the relationship given in the text. Red (plus signs), green (crosses), and blue (asterisks) symbols represent values calculated with the direct, strain-fluctuation, and stress-fluctuation methods, respectively. The dotted line represents the experimentally determined values [1].

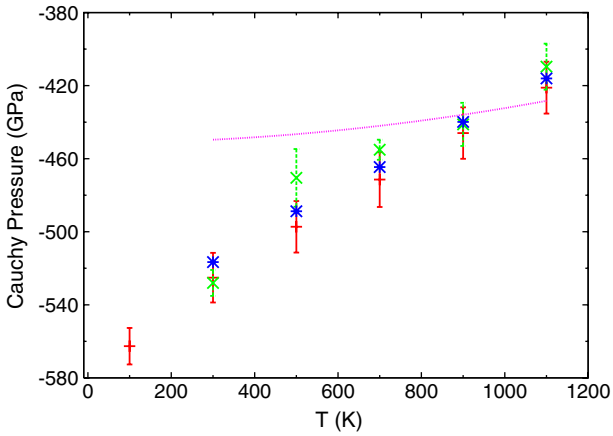

Figure 8. Cauchy pressure of diamond as a function of temperature. Pressures are calculated from the calculated elastic constants using the relationship given in the text. Red (plus signs), green (crosses), and blue (asterisks) symbols represent values calculated with the direct, strain-fluctuation, and stress-fluctuation methods, respectively. The dotted line represents the experimentally determined values [1].

method is more difficult to implement because it requires the analytic second derivative of the potential energy function with respect to strain. For potential energy functions with complicated functional forms, this term can be difficult to obtain. Both of these methods can also be applied to amorphous hydrocarbon systems. For a crystalline material such as diamond, it is also possible to calculate the elastic constants at non-zero temperatures by making the proper deformations to an orthorhombic simulation cell. While this method is more cumbersome than the fluctuation methods, it provided additional data points for the diamond system.

The second-generation REBO potential has been previously shown to accurately predict the 0 K elastic constants of diamond and graphite [37]. In this work, the non-zero temperature

elastic constants, the bulk modulus, the thermal expansion coefficient, and the Cauchy pressure of diamond between 100 and 1100 K have been calculated.

Due to the inability of classical MD simulations to accurately predict the thermal expansion at low temperatures, as well as the high Debye temperature of diamond, the calculated elastic constants exhibit a faster softening trend than the experimental values. However, the second-generation REBO potential does reproduce the correct qualitative trends in the bulk modulus and in two of diamond's elastic constants with temperature. In addition, it correctly predicts that diamond has a negative Cauchy pressure in the temperature range examined. Thus, the second-generation REBO potential can be used to make qualitative predictions about the changes in material and tribological properties of hydrocarbon systems with changing temperature.

It is clear that the revised functional form of the second-generation REBO is key to its success in producing the correct qualitative trends in the reported material properties with temperature. No effort was made to fit the 0 K elastic constants of diamond or graphite in the original REBO potential [48]. In fact, Brenner and co-workers determined that it was not possible to adequately reproduce all the 0 K elastic constants with the original functional form. As a result, the functional form of the REBO potential was revised when 'fitting' the second-generation REBO [37]. Subsequent examination of the original REBO potential revealed that it does not reproduce the correct qualitative trends in the elastic constants of diamond with temperature [79]. This is also the case for potentials that share the original REBO formalism such as, Dyson and Smith's C–Si–H potential [80], the GEEBOD potential [81], the Si–H potential of Ramana Murty [82], and the modified XB-potential of Sbraccia *et al* [83].

In principle, it is should possible to obtain more accurate data at non-zero temperatures using the second-generation REBO formalism. However, because force constants depend on temperature, the parameters of such a potential would have to be functions of temperature. Thus, it would be possible to have high-temperature parameters for a potential. Such a potential would be useful in Monte Carlo simulations or in MD simulations where the temperature is constant and in the range where the potential was fit.

Acknowledgments

This work was supported by The Air Force Office of Scientific Research (F1ATA04295G001 and F1ATA04295G002) and The Office of Naval Research (N00014-06-WR-20205).

References

[1] Zouboulis E S, Grimsditch M, Ramdas A K and Rodriguez S 1998 *Phys. Rev.* B **57** 2889–96
[2] Erdemir A and Donnet C 2001 *Modern Tribology Handbook* (Boca Raton, FL: CRC Press LLC) chapter (Tribology of Diamond, Diamond-Like Carbon, and Related Films) pp 871–908
[3] Lide D R (ed) 1992 *CRC Handbook of Chemistry and Physics* 71st edn (Boca Raton, FL: CRC Press)
[4] Gruen D M 2001 *Mater. Res. Soc. Bull.* **26** 771–6
[5] Grill A 1997 *Surf. Coat. Technol.* **94/95** 507–13
[6] Robertson J 1992 *Surf. Coat. Technol.* **50** 185–203
[7] Riedo E, Chevrier J, Comin F and Brune H 2001 *Surf. Sci.* **477** 25–34
[8] Riedo E, Levy F and Brune H 2002 *Phys. Rev. Lett.* **88** 185505
[9] Heimberg J A, Wahl K J, Singer I L and Erdemir A 2001 *Appl. Phys. Lett.* **78** 2449–51
[10] Fontaine J, Donnet C, Grill A and LeMogne T 2001 *Surf. Coat. Technol.* **146/147** 286–91
[11] Erdemir A, Fenski G R, Krauss A R, Gruen D M, McCauley T and Csencsits R T 1999 *Surf. Coat. Technol.* **120/121** 565–72
[12] Donnet C and Grill A 1997 *Surf. Coat. Technol.* **94/95** 456–62
[13] Huu T L, Schmitt M and Paulmier D 1999 *Surf. Sci.* **433–435** 690–5
[14] Forbes I S, Rabeau J R, Wilson J I B and John P 2003 *Mater. Sci. Technol.* **19** 553–6
[15] Forbes I S and Wilson J I B 2002 *Thin Solid Films* **420** 508–14

[16] Robertson J 2003 *Diamond Relat. Mater.* **12** 79–94
[17] Webster J R, Dyck C W, Sullivan J P, Friedmann T A and Carton A 2004 *Electron. Lett.* **40** 43–53
[18] Hayward I P, Singer I L and Seitzman L E 1992 *Wear* **157** 215–27
[19] Hayward I P 1991 *Surf. Coat. Technol.* **49** 554–9
[20] Gao G T, Mikulski P T, Chateauneuf G M and Harrison J A 2003 *J. Phys. Chem.* B **107** 11082–90
[21] Gao G T, Mikulski P T and Harrison J A 2002 *J. Am. Chem. Soc.* **124** 7202–9
[22] Harrison J A, White C T, Colton R J and Brenner D W 1992 *Phys. Rev.* B **46** 9700–8
[23] Harrison J A and Brenner D W 1994 *J. Am. Chem. Soc.* **116** 10399–402
[24] Perry M D and Harrison J A 1995 *J. Phys. Chem.* **99** 9960–5
[25] Perry M D and Harrison J A 1995 *Langmuir* **12** 19
[26] Perry M D and Harrison J A 1995 *Tribol. Lett.* **1** 109–19
[27] Perry M D and Harrison J A 1996 *Thin Solid Films* **290/291** 211–5
[28] Perry M D and Harrison J A 1997 *J. Phys. Chem.* B **101** 1364–73
[29] Harrison J A and Perry S S 1998 *MRS Bull.* **23** 27–31
[30] Zhao Y P, Wang L S and Yu T X 2003 *J. Adhes. Sci. Technol.* **17** 519–46
[31] Tang W C and Lee A P 2001 *Mater. Res. Soc. Bull.* **26** 318–9
[32] deBoer M P and Mayer T M 2001 *Mater. Res. Soc. Bull.* **26** 302–4
[33] Maboudian R and Howe R T 1997 *J. Vac. Sci. Technol.* B **15** 1–20
[34] Houston M R, Howe R T, Komvopoulos K and Maboudian R 1995 *Mater. Res. Soc. Symp. Proc.* **383** 391–402
[35] Kohn E, Gluche P and Adamschik M 1999 *Diamond Relat. Mater.* **8** 934–40
[36] Sprik M, Impey R W and Klein M L 1984 *Phys. Rev.* B **29** 4368–74
[37] Brenner D W, Shenderova O A, Harrison J A, Stuart S J, Ni B and Sinnott S B 2002 *J. Phys.: Condens. Matter* **14** 783–802
[38] Brenner D W 2000 *Phys. Status Solidi* b **217** 23
[39] Lovett D R 1989 *Tensor Properties of Crystals* (Bristol: Hilger)
[40] Ray J R 1988 *Comput. Phys. Rep.* **8** 109–51
[41] Parrinello M and Rahman A 1982 *J. Chem. Phys.* **76** 2662–6
[42] Ray J R 1982 *J. Appl. Phys.* **53** 6441–3
[43] Ray J R and Rahman A 1984 *J. Chem. Phys.* **80** 4423–8
[44] Ray J R and Rahman A 1985 *J. Chem. Phys.* **82** 4243–7
[45] Ray J R, Moody M C and Rahman A 1985 *Phys. Rev.* B **32** 733–5
[46] Lutsko J F 1989 *J. Appl. Phys.* **65** 2991–7
[47] Yoshimoto K, Papakonstantopoulos G J, Lutsko J F and dePablo J J 2005 *Phys. Rev.* B **71** 184108
[48] Brenner D W 1990 *Phys. Rev.* B **42** 9458–71
[49] Brenner D W, Harrison J A, Colton R J and White C T 1991 *Thin Solid Films* **206** 220–3
[50] Garrison B J, Dawnkaski E J, Srivastava D and Brenner D W 1992 *Science* **255** 835–8
[51] Harrison J A, Stuart S J, Robertson D H and White C T 1997 *J. Phys. Chem.* B **101** 9682–5
[52] Robertson D, Brenner D and Mintmire J 1992 *Phys. Rev.* B **45** 12592–5
[53] Brenner D, Dunlap B I, Harrison J A, Mintmire J W, Mowrey R C, Robertson D H and White C T 1991 *Phys. Rev.* B **44** 3479–82
[54] Mowrey R C, Ross M M and Callahan J H 1992 *J. Phys. Chem.* **96** 4755–61
[55] Qi L F and Sinnott S B 1998 *Surf. Sci.* **398** 195–202
[56] Garg A and Sinnott S B 1998 *Chem. Phys. Lett.* **295** 273–8
[57] Garg A, Han J and Sinnott S B 1998 *Phys. Rev. Lett.* **81** 2260–3
[58] Shenderova O, Brenner D W and Yang L H 1999 *Phys. Rev.* B **60** 7043–52
[59] Shenderova O and Brenner D W 1999 *Phys. Rev.* B **60** 7053–61
[60] Shenderova O and Brenner D W 2002 *Mater. Solid State Phenom.* **87** 205–13
[61] Squire D R, Holt A C and Hoover W G 1969 *Physica* **42** 388–97
[62] Wolf R J, Mansour K A, Lee M W and Ray J R 1992 *Phys. Rev.* B **46** 8027–35
[63] Fay P J and Ray J R 1992 *Phys. Rev.* A **46** 4645–9
[64] Karimi M, Yates H, Ray J R, Kaplan T and Mostoller M 1998 *Phys. Rev.* B **58** 6019–25
[65] Sengupta S, Nielaba P, Rao M and Binder K 2000 *Phys. Rev.* E **61** 1072–80
[66] VanWorkum K and dePablo J 2003 *Phys. Rev.* E **67** 011505
[67] Yoshimoto K, Jain T S, Workum K V, Nealey P F and dePablo J 2004 *Phys. Rev. Lett.* **93** 175501
[68] Parrinello M and Rahman A 1980 *Phys. Rev. Lett.* **45** 1196–9
[69] Van Workum K, Gao G T, Schall J D and Harrison J A 2005 *Phys. Rev.* B in preparation
[70] Gear C W 1971 *Numerical Initial Value Problems in Ordinary Differential Equations* (Englewood Cliffs, NJ: Prentice-Hall)

[71] Nose S 1984 *Mol. Phys.* **52** 255–68
[72] Andersen H C 1980 *J. Chem. Phys.* **72** 2384–93
[73] Thewlis J and Davey A R 1956 *Phil. Mag.* **1** 409–14
[74] Barron T H K, Collins J G and White G K 1980 *Adv. Phys.* **29** 609–730
[75] Nose S and Klein M L 1983 *Mol. Phys.* **50** 1055–76
[76] Gusev A A, Zehnder M M and Suter U W 1996 *Phys. Rev.* B **54** 1–4
[77] Stuart S J, Tutein A B and Harrison J A 2000 *J. Chem. Phys.* **112** 6472–86
[78] Yates B 1972 *Thermal Expansion* (New York: Plenum)
[79] Schall J D, Van Workum K, Gao G T and Harrison J A 2005 in preparation
[80] Dyson A and Smith P 1996 *Surf. Sci.* **355** 140–50
[81] Che J C, Cagin T and Goddard W A III 1999 *Theor. Chem. Acc.* **102** 346
[82] Murty M V R and Atwater H A 1995 *Phys. Rev.* B **51** 4889–93
[83] Sbraccia C, Silvestrelli P L and Ancilotto A F 2002 *Surf. Sci.* **516** 147